

1 **Measurement Report: Rapid changes of chemical characteristics and health risks for high**
2 **time-resolved trace elements in PM_{2.5} in a typical industrial city in response to stringent**
3 **clean air actions**

4 Rui Li^{a*}, Yining Gao^a, Yubao Chen^a, Meng Peng^{b,c*}, Weidong Zhao^{c*}, Gehui Wang^a, Jiming Hao^b

5 ^a *Key Laboratory of Geographic Information Science of the Ministry of Education, School of*
6 *Geographic Sciences, East China Normal University, Shanghai, 200241, P.R. China*

7 ^b *State Key Joint Laboratory of Environment Simulation and Pollution Control, School of*
8 *Environment, Tsinghua University, Beijing, 100084, P.R. China*

9 ^c *Institute of Energy ~~conservation~~ Conservation and Environmental Protection, China Electronic*
10 *Information Industry Development Research Institute, Beijing, 100084, P.R. China*

11 *** Correspondence to:**

12 Prof. Li (rli@geo.ecnu.edu.cn), Dr. Peng (mvponesky@163.com), and Prof. Zhao

13 (zhaoweidong@ccidthinktank.com)

14 **Abstract**

15 Atmospheric trace metals entail significant damages in human health and ecosystem safety, and thus
16 a series of clean air actions have been implemented to decrease the ambient element concentrations.
17 Unfortunately, the impact of these emission control measures on element concentrations in fine
18 particles remains poorly understood. In our study, the random forest (RF) model was applied to
19 distinguish the effects of emission and meteorology to trace elements in PM_{2.5} in a typical industrial
20 city named Tangshan based on a three-year (2017-2020) hourly field observation. The result
21 suggested that the clean air actions have facilitated the dramatic decreases of the deweathered
22 concentrations of Ga, Co, Pb, Zn, and As by 72%, 67%, 62%, 59%, and 54%, respectively. It is
23 attributable to the strict implementation of “coal to gas” strategies and optimization of industrial
24 structure and layout. However, the deweathered levels of Ca (8.3%), Cr (18.5%), and Fe (23%) only
25 displayed minor decreases, indicating that the emission control measures for ferrous metal smelting
26 and vehicle emission were not very effective. The positive matrix factorization (PMF) results
27 suggested that the contribution ratios of biomass burning, non-ferrous metal smelting, coal

28 combustion, ferrous metal smelting, heavy oil combustion, and traffic-related dust changed from
29 33%, 11%, 15%, 13%, 3%, and 25% to 33%, 8%, 8%, 13%, 4%, and 33%, respectively. To date,
30 no significant noncarcinogenic and carcinogenic risks were observed for all of the elements, while
31 both of As and Pb still showed relatively high health damages. It was proposed to further cut down
32 the combustion-related emissions (e.g., As and Pb) because it showed the highest marginal health
33 benefits. Besides, the control of traffic-related emissions might be a key abatement strategy to
34 facilitate the reduction of elements in fine particles.

35 **Keywords:** hourly trace elements; chemical characteristics; health risks; clean air actions; Tangshan

36 1. Introduction

37 Along with the rapid economic development and accelerated urbanization, the energy
38 consumption and output of various industrial products worldwide displayed persistent increases,
39 thereby leading to massive emissions of elements especially trace metals into the atmosphere (Tian
40 et al., 2015; Zhu et al., 2020). These elements injected into the atmosphere could pose great threat
41 to the terrestrial and aquatic ecosystem via dry/wet deposition and then endanger human health
42 through the physicochemical transfer and bioaccumulation in food chains (Fernandez et al., 2000;
43 Harmens et al., 2010; Storelli, 2008). For instance, some toxic trace metals including cadmium (Cd),
44 lead (Pb), and mercury (Hg) were often regarded as human carcinogens even in trace amounts
45 (Micheline et al., 2019; Olujimi et al., 2015). Besides, the excessive accumulation of some
46 biological essential elements such as copper (Cu), iron (Fe), and zinc (Zn) could initiate activation
47 of inflammatory cascades in tissues and the induction of biochemical synthesis pathways by
48 catalyzing the generation of reactive oxygen species (ROS) (Alies et al., 2013; Lopez-Cruz et al.,
49 2016; Saffari et al., 2014), though minor enrichment of these elements was beneficial to the human
50 health and plant growth (Oldani et al., 2017). Apart from the health impacts, some transition metals
51 (e.g., Ni, Zn) could catalyze some chemical reactions such as particle-phase sulfate generation and
52 heterogeneous production and removal of gas-phase hydrogen oxide radicals (HO_x) to aggravate the
53 haze formation (Clements et al., 2013; Guo et al., 2014). Therefore, it is highly imperative to
54 recognize the pollution status of elements in the atmosphere, to identify the major sources and then
55 to propose effective control measures to alleviate their negative effects on air pollution and human
56 health especially in some developing countries.

57 In the past decades, hundreds of studies investigated the pollution levels of elements and
58 revealed their sources in various study regions including urban (Das et al., 2018; Duan and Tan,
59 2013; Lyu et al., 2017; Grivas et al., 2018; Clements et al., 2014), marine (Shi et al., 2015; Witt et
60 al., 2006), mountainous (Kang et al., 2016). Most of these studies used filter sampling (one sample
61 or two samples each day) coupled with offline analysis using inductively coupled plasma mass
62 spectrometry (ICP-MS) or inductively coupled plasma-atomic emission spectrometry (ICP-AES) to
63 determine the element concentrations in the atmosphere (Ao et al., 2019; Lin et al., 2016). Although
64 these studies have obtained much valuable information about the occurrence levels and key sources
65 of ambient elements, the low time-resolution data cannot accurately reflect the dynamic
66 transformation and evolution of ambient elements. It was well known that atmospheric emissions,
67 transport and deposition significantly relied on rapidly evolving meteorological conditions (Holden
68 et al., 2016; Rasmussen, 1998), and thus the offline samples inevitably ignored the impacts of
69 environmental shifts with rapid temporality on the atmospheric element concentrations. Moreover,
70 most of current source apportionment studies employed receptor models (positive matrix
71 factorization (PMF)) to determine the potential sources of elements (Jeong et al., 2016; Lyu et al.,
72 2017), and the accuracy of these models was strongly dependent on the sample size and time
73 resolution (Liu et al., 2018b). In this regard, the high time-resolved observation of atmospheric
74 elements provided an unprecedented opportunity to characterize the occurrence levels, identify their
75 major sources, and assess the health impacts.

76 To date, only a few studies applied the high-resolution devices to capture the hourly variability
77 of ambient elements. Prati et al. (2000) firstly used Particle Induced X-ray Emission (PIXE)
78 measurements to measure hourly trace elements in Genoa in Italy. Following this work,
79 D'Alessandro et al. (2003) and Dall'Osto et al. (2013) also employed the same technique to
80 determine the trace metals in Italian towns and Barcelona, respectively. Later on, Jeong et al. (2016)
81 used the Xact metals monitor to reveal the temporal variability of atmospheric elements in Toronto,
82 Canada in summer and winter during 2013-2014. Recently, the Xact metals monitor has begun to
83 be employed in China due to the higher accuracy and convenience. Chang et al. (2018) firstly used
84 the online multi-element analyzer to achieve a one-year near real-time observation of ambient
85 elements in China and found that traffic, nonferrous metal smelting and coal combustion were major

86 sources of atmospheric trace metals. Afterwards, Cui et al. (2019) applied the analyzer to monitor
87 atmospheric elements during a full year, and demonstrated that dust, industry, and biomass burning
88 were the dominant sources of most trace elements in Beijing, accounting for 36%, 10.7%, and 27%
89 of total PM_{2.5} concentration, respectively. Up to date, continuous hourly element observation was
90 only performed less than one year in most of the previous studies, and the long-term temporal
91 variability of absolute concentrations and key pollution sources of atmospheric elements cannot be
92 fully revealed.

93 Since 2013, Chinese government proposed a strict Air Pollution Prevention and Control Action
94 Plan (the Action Plan) across China and the emissions of multiple gaseous pollutants showed
95 significant decreases (Ma et al., 2019; Li et al., 2021a). In turn, the absolute concentrations and
96 health effects of air pollutants also experienced the rapid changes due to these stringent control
97 measures. Zhang et al. (2019) reported that the population-weighted annual mean PM_{2.5}
98 concentration decreased from 62 to 42 µg/m³ during 2013-2017 and reduced PM_{2.5}-attributable
99 premature deaths by 0.4 million due to the impact of the Action Plan. Shortly after that, Geng et al.
100 (2019) estimated that the population-weighted mean concentrations of SO₄²⁻, NO₃⁻, and NH₄⁺ in
101 PM_{2.5} decreased from 11.1, 13.8, and 7.4 µg/m³ to 6.7, 13.1, and 5.8 µg/m³, respectively, during the
102 same period. Nevertheless, the impact of the Action Plan on trace elements in fine particles still
103 remained poorly understood. Especially, the knowledge about the variation of source apportionment
104 and health risks for trace elements response to the Action Plan was extremely limited. Moreover,
105 most of the previous studies only utilized the original concentrations to analyze the impact of the
106 clean air policy (He et al., 2021; Xiao et al., 2020). It was well known that the pollutant
107 concentrations in the atmosphere were affected by meteorology and anthropogenic emissions
108 simultaneously (Li et al., 2021b), and the use of original element concentrations alone cannot assess
109 the unique contribution of emission reduction to the air pollutants. Thus, it is urgently needed to
110 remove the effect of meteorology and accurately capture the independent influence of the Action
111 Plan on the chemical characteristics, source apportionment, and health risks of trace elements. Such
112 knowledge is critical to design effective air pollution mitigation strategies in the near future.

113 As a heavily industrialized city located in the North China Plain (NCP), Tangshan possesses
114 many energy-intensive industries including coal-fired power plants, non-ferrous smelting industries,

115 textiles, building materials, chemical engineering, and papermaking industries (Ren et al., 2011).
116 Intensifying industrial development and urbanization aggravated local air quality. Previous studies
117 performed in Tangshan focused on the trace metals in soils and dusts (Cui et al., 2020; Song et al.,
118 2011), whereas no study analyzed the long-term and high-resolution variabilities of atmospheric
119 elements. Since 2013, many emission control measures such as the establishment of desulfurization
120 and denitration facilities for the coal-fired power sector have been strictly implemented in Tangshan
121 (Ma et al., 2019). Especially after 2017, the coal to gas project has started to be implemented in
122 Tangshan and the energy structure underwent significant change (Wang et al., 2020b). In response
123 to substantial pollution control policies, the chemical compositions and major sources of trace
124 elements might show corresponding change. Here, we conducted a near real-time measurement of
125 atmospheric elements in PM_{2.5} using a Xact multi-metals analyzer in Tangshan, China, during
126 September 2017 to August 2020. The primary objectives of our study were to (1) determine the
127 occurrence levels of elements in PM_{2.5} of Tangshan; (2) to analyze the seasonal and intra-week
128 variations of atmospheric elements and to distinguish the separate contributions of emission and
129 meteorology to these species; (3) to quantify the changes of major sources for atmospheric elements
130 during this period; (4) to assess the changes of health risks in response to these pollution control
131 measures.

132 **2. Material and methods**

133 2.1 Sampling site

134 The sampling site (39.66°N, 118.18°E) is situated on the rooftop (~20 m above the ground) of a
135 building in the urban district of Tangshan and no high buildings spread around within 100 m range.
136 The sampling site is close to some major roads including the Airport Road, Huayan North Road,
137 and Changhong Road. A large number of commercial streets and recreation facility surround the
138 site. Although no big industrial point source was closely adjacent to the sampling site, many
139 potential pollution sources were located more than 15 km away from the site. For instance, the Beihu
140 industrial region is located about 15 km in the eastern direction of the site. Some large iron steel
141 industries and nonferrous/ferrous smelting industries were located on the north of sampling site
142 (more than 30 km). Besides, most of the large petrochemical industries, coal-fired power plants, and
143 shipping industries focus on the Caofeidian and Haigang developing zones, both of which were

144 located about 50 km in the South area of the sampling site. The detailed location is depicted in
145 Figure 1.

146 2.2 Instrumentation

147 Hourly mass concentrations of 22 elements, including Ag, As, Au, Ca, Co, Cu, Cd, Cr, Fe, Ga,
148 Hg, K, Mn, Ni, Pb, Pd, Sb, Se, Sn, Tl, V, and Zn in PM_{2.5} were determined continuously by an online
149 multi-element analyzer (Model Xact 625, Cooper Environment Service, USA) (Table S1). The
150 sample air is drawn through a small spot on the tape where the PM_{2.5} was collected at a flow rate of
151 16.7 L min⁻¹ during September 2017-August 2020. An internal Pd pod is utilized as an internal
152 standard to determine the stability of the instrument. Tl was removed from the datasets because over
153 95% of their concentrations were below the limit of detection (LOD) (Table S2). Au, Cd, Sn and Sb
154 were also excluded from the datasets because over 50% of the concentrations for these metals were
155 below the LOD. To validate the reliability of the online multi-element analyzer, many previous
156 studies used the filter sampling coupled with ICP-MS and ICP-AES to determine the daily
157 concentrations of elements and confirmed that the online device showed good agreement with the
158 filter sampling (Furger et al., 2017; Tianxue et al., 2006). Hourly averaged meteorological
159 parameters including air temperature (T), relative humidity (RH), air pressure (P), wind direction
160 (WD), and wind speed (WS) during the sampling period were measured by a weather station with
161 sonic anemometer (150WX, Airmar, Milford, NH, USA). The hourly mass concentration of PM_{2.5}
162 was determined by a particulate monitor (Thermo, FH62C-14). The routine procedures, including
163 the daily zero or standard calibration, span and range check, station environmental control and staff
164 certification, followed the Technical Guideline of Automatic Stations of Ambient Air Quality in
165 Tangshan based on the national specification HJ/T193-2005, which was revised based on the
166 technical guidance established by the US EPA. Quality Assurance and Quality Control (QA/QC) for
167 the Xact measurements was implemented throughout the sampling period. The internal Pd upscale
168 value was recorded after daily programmed test for the instrument.

169 2.3 Deweathered model development

170 The concentrations of air pollutants were affected by meteorological parameters and emissions
171 simultaneously. In order to separate the contributions of emissions, the impacts of meteorological
172 conditions must be eliminated. In this study, a typical machine-learning model named random forest

173 (RF) approach was applied to distinguish the effects of emissions and meteorological conditions
174 (Chen et al., 2018). All trace elements in PM_{2.5} were treated as the dependent variables. The time
175 predictors (year, day of year (DOY), day of week (DOW), hour of day (HOY)) and meteorological
176 factors including air temperature (T), relative humidity (RH), wind speed (WS), wind direction
177 (WD), and air pressure (P) were regarded as the predictors (Figure S1). The original dataset was
178 randomly classified into a training dataset (80% of input dataset) for developing the RF model and
179 the ~~remained-remaining~~ one was treated as the test dataset. After the building of the RF model, the
180 deweathered technique was employed to predict the concentrations of trace elements at a specific
181 time point. The deweathered element concentrations served as the concentrations contributed by
182 emission alone. The differences between the original element concentrations and the deweathered
183 element concentrations were regarded as the concentrations contributed by meteorology. Many
184 statistical indicators including R² value, root-mean-square error (RMSE), and mean absolute error
185 (MAE) were regarded as the major indicators to evaluate the RF modelling accuracy. The RF model
186 with the 5-fold cross-validation R² value less than 0.5 was considered to be an unconvincing result
187 and cannot reflect the impacts of emission and meteorology on air pollutants accurately because
188 more than 50% variability of the training model cannot be appropriately explained. After the model
189 evaluation, only the trace elements with the cross-validation R² values larger than 0.5 were selected
190 to estimate the respective contributions of emission and meteorology to the total element
191 concentrations.

192 2.4 PMF model

193 As a typical receptor model applied to source apportionment, the PMF 5.0 version was used to
194 identify the major origins of the atmospheric elements and to determine the contribution ratio of
195 each source to these elements (Norris et al., 2014). The objective of PMF is to solve the issues of
196 chemical mass balance between the measured concentration of each element and its source
197 contributions by decomposing the input matrix into factor contributions and factor profiles. The
198 detailed equation is shown in Eq. (1). Besides, the contribution of each source for an individual
199 element must be non-negative because no sample has a negative source contribution. In brief, the
200 basic principle of PMF is to calculate the least object function Q when the g_{ik} must be a positive-
201 definite matrix based on Eq. (2) (Paatero and Tapper, 1994; Reff et al., 2007).

202

$$x_{ij} = \sum_{k=1}^p g_{ik} f_{kj} + e_{ij} \quad (1)$$

203

$$Q = \sum_{i=1}^n \sum_{j=1}^m \left[\frac{x_{ij} - \sum_{k=1}^p g_{ik} f_{kj}}{u_{ij}} \right]^2 \quad (2)$$

204

where x_{ij} and e_{ij} denote the concentration and uncertainty of the j th element, respectively. g_{ik}

205

represents the contribution ratio of the k th source to the i th sample, f_{kj} represents the ratio of the j th

206

element in the k th source, and e_{ij} indicates the residual of the j th element in the i th sample. The

207

uncertainties associated with factor profiles were evaluated using three error calculation methods

208

including the bootstrap (BS) method, displacement (DISP) analysis, and the combination method

209

of DISP and BS (BS-DISP). For the BS method, 100 runs were performed and the result has been

210

believed to be valid since all of the factors showed a mapping of above 90%. DISP analysis also

211

confirmed that the solution was considered to be stable because the observed drop in the Q value

212

was less than 0.1% and no factor swap occurred. For the BS-DISP analysis, the solution has been

213

verified to be useful because the observed drop in the Q value was less than 0.5%. Furthermore,

214

both of the results from BS and BS-DISP did not suggest any asymmetry or rotational ambiguity

215

for all of the factors (Manousakas et al., 2017; Taghvaei et al., 2018).

216

2.5 Health risk assessment of trace metals in PM_{2.5}

217

As a typical industrial city, Tangshan possesses a large number of residents and poor air quality.

218

Therefore, the residents in Tangshan might suffer from severe exposure risks of trace metals. In our

219

work, the carcinogenic and non-carcinogenic risks of trace metals in PM_{2.5} were evaluated based on

220

some statistical threshold proposed by the International Agency for Research on Cancer (IARC).

221

Based on the criterion of the IARC, As, Ni, Cr, and Pb were considered to be carcinogenic to humans.

222

The carcinogenic and non-carcinogenic risks induced by metal exposure for adults and children

223

were evaluated based on the carcinogenic risks (CR) and hazard quotient (HQ). The formulas for

224

calculating ADD, CR, and HQ are as follows:

225

$$ADD = (C \times InhR \times EF \times ED) / (BW \times AT) \quad (3)$$

226

$$HQ = ADD / RfD \quad (4)$$

227

$$CR = ADD \times CSF \quad (5)$$

228

where C (mg m^{-3}) denotes the concentration of the corresponding trace metal in PM_{2.5}; $InhR$ is the

设置了格式: 上标

设置了格式: 上标

229 respiratory rate ($\text{m}^3 \text{d}^{-1}$); EF represents the annual exposure frequency (d y^{-1}); ED is the exposure
230 duration (year); BW is the average body weight (kg); AT denotes the average exposure time (d);
231 ADD means the daily intake (mg/kg/day) of trace metals; RfD represents the reference dose (mg
232 $\text{kg}^{-1} \text{d}^{-1}$), calculated with reference concentrations; CSF is the cancer slope factor (kg d mg^{-1}). The
233 potential non-carcinogenic risk of the trace metal might be high when HQ was above 1.0, whereas
234 the health risk is not obvious when HQ is below 1.0. The carcinogenic risk of each trace metal is
235 evaluated based on whether CR is higher than 10^{-4} .

236 3. Results and discussion

237 3.1 Occurrence levels and inter-annual variations of original element concentrations

238 The total mass concentrations of 16 elements in $\text{PM}_{2.5}$ of Tangshan varied between 230 ng/m^3
239 to 20000 ng/m^3 , with the average value (\pm standard deviation) of $3100 \pm 900 \text{ ng/m}^3$. The total
240 element concentrations in Tangshan accounted for 5.7% of the total mass concentrations of $\text{PM}_{2.5}$,
241 which was slightly higher than those in Beijing (4.7%) and Qingdao (4.0%), and significantly higher
242 than that in Shanghai (1.80%) (Chang et al., 2018; Cui et al., 2019). As depicted in Figure 2, the
243 **average concentrations (\pm standard deviation) concentrations** of these elements followed the order
244 of $\text{K} (1400 \pm 950 \text{ ng/m}^3) > \text{Fe} (880 \pm 590 \text{ ng/m}^3) > \text{Ca} (330 \pm 270 \text{ ng/m}^3) > \text{Zn} (320 \pm 160 \text{ ng/m}^3) >$
245 $\text{Pb} (58 \pm 36 \text{ ng/m}^3) > \text{Mn} (54 \pm 32 \text{ ng/m}^3) > \text{Cu} (22 \pm 19 \text{ ng/m}^3) > \text{As} (15.3 \pm 11.0 \text{ ng/m}^3) > \text{Se} (6.5$
246 $\pm 5.3 \text{ ng/m}^3) > \text{V} (4.0 \pm 3.6 \text{ ng/m}^3) > \text{Cr} (2.8 \pm 2.2 \text{ ng/m}^3) > \text{Ag} (2.8 \pm 2.1 \text{ ng/m}^3) > \text{Ni} (2.2 \pm 1.8$
247 $\text{ ng/m}^3) > \text{Hg} (1.5 \pm 0.8 \text{ ng/m}^3) > \text{Ga} (0.9 \pm 0.7 \text{ ng/m}^3) > \text{Co} (0.7 \pm 0.2 \text{ ng/m}^3)$. Among all of these
248 elements, K, Fe, Zn, and Ca were the most abundant species, accounting for 95% of the total
249 elements in $\text{PM}_{2.5}$. The remaining element concentrations only accounted for less than 6% of the
250 total element concentrations, which was similar to in previous studies (Chang et al., 2018; Cui et al.,
251 2019). Nearly all of the trace elements in Tangshan, Beijing, Qingdao, and Shanghai were
252 significantly lower than those in Zibo during 2006-2007 (Table S3). It suggested that the trace
253 elements in China experienced marked decreases in the past decades (Zhang et al., 2018). Compared
254 with some cities in some developed countries, all of the trace element concentrations were
255 significantly higher than those in London and Toronto. Moreover, the concentrations of K, Ca, V,
256 Cr, Mn, and Fe in Tangshan were higher than those in Venice, Italy.

257 Due to the higher exposure risk and great threat to human health, it is necessary to compare the

258 trace metal concentrations with the risk threshold proposed by many organizations or countries. As
259 shown in Table 1, we have collected many risk thresholds in different countries and found that the
260 Hg ($1.5 \pm 0.8 \text{ ng/m}^3$), Ni ($2.2 \pm 1.8 \text{ ng/m}^3$), and Pb concentrations ($58 \pm 36 \text{ ng/m}^3$) in Tangshan were
261 significantly lower than the thresholds of the Chinese Ambient Air Quality Standard (CAAQS) (Hg:
262 50 ng/m^3), World Health Organization (WHO) (Hg: 1000 ng/m^3 , Ni: 25 ng/m^3 , and Pb: 1000 ng/m^3),
263 European Union (EU) (Ni: 20 ng/m^3), and the United States (Pb: 150 ng/m^3). However, both of the
264 As ($15 \pm 11 \text{ ng/m}^3$) and Cr concentrations ($2.8 \pm 2.2 \text{ ng/m}^3$) in PM_{2.5} of Tangshan were much higher
265 than the standard values of the CAAQS (As: 6.0 ng/m^3 and Cr: 0.03 ng/m^3), WHO (As: 6.6 ng/m^3
266 and Cr: 0.25 ng/m^3), and EU (As: 6.0 ng/m^3).

267 The inter-annual variation of the original concentrations of the trace elements in PM_{2.5} are
268 depicted in Figure 3 and S2-S3. The original concentrations of all the trace elements exhibited
269 decreasing trends. The Cu, Co, Zn, Pb, As, and Ga concentrations showed dramatic decreases from
270 37 to 12 ng/m^3 (68%), 1.21 to 0.4 ng/m^3 (66%), 400 to 190 ng/m^3 (53%), 71 to 40 ng/m^3 (44%), 20
271 to 11 ng/m^3 (44%), and 1.09 to 0.6 ng/m^3 (42%), respectively. Following these species, the K (40%),
272 Ag (39%), V (39%), Ni (36%), Ca (33%), Mn (29%), Se (29%), Fe (27%), and Cr (21%)
273 concentrations showed moderate decreasing ratios. The observed Hg level exhibited the lowest
274 decreasing ratio from 1.59 to 1.43 ng/m^3 (9.9%).

275 3.2 Impact of emission reduction on trace element concentrations

276 Although the original concentrations of the trace elements could be utilized to analyze the impact
277 of the clean air policy, the role of emission reduction on the element concentration might not be
278 clearly clarified because the meteorological factors were also important variables affecting the air
279 quality. In order to accurately reflect the response of the element concentrations to the emission
280 reduction alone during 2017-2020, the meteorological conditions were eliminated by the RF model
281 in our study. Based on the results in Figure S4, the RF models for all of the species showed better
282 performance because their R² values were higher than 0.50, and the slopes of all of the fitting curves
283 were also close to the R² values. The result suggested that the separation of meteorology and
284 emission of trace elements based on the RF model was reliable. During 2017-2020, the deweathered
285 concentrations of Ga, Co, Pb, Zn, and As showed the rapid decreases from 1.52 to 0.4 ng/m^3 (72%),
286 1.31 to 0.4 ng/m^3 (67%), 92 to 35 ng/m^3 (62%), 410 to 170 ng/m^3 (59%), and 21 to 10 ng/m^3 (54%),

287 respectively (Figure 3). It was well known that As, Co, and Pb were typical marker elements for
288 coal combustion and the “coal-to-gas” and “coal-to-electricity” strategies have been widely
289 performed in Tangshan (Fang et al., 2020; Li et al., 2017). Wang et al. (2020a) have estimated that
290 these effective control measures have contributed to around 60% of the total PM_{2.5} reductions.
291 Meanwhile, the upgradation and optimization of the industrial structure/layout and the shutdown of
292 high-pollution industries were also strictly implemented in Tangshan, and thus led to the dramatic
293 decreases of Ga and Zn concentrations because Ga and Zn were common forms of nonferrous metal
294 smelting (Tian et al., 2015). In contrast, the deweathered Ca level displayed the lowest decrease
295 ratio (8.3%) from 2017 to 2020, indicating that clean air actions cannot significantly reduce the
296 fugitive emissions. In addition, the deweathered Fe (23%) and Cr (18.5%) also suffered from
297 relatively low decrease ratios. It was well documented that Fe and Cr originated from metallurgical
298 industry such as steel production and ferrous metal smelting (Tian et al., 2015), and the slight
299 decreases of the deweathered Fe and Cr levels during the sampling period suggested that the
300 emission control measures for ferrous metal smelting should be strengthened in the future.

301 In addition, the decreasing ratios of the deweathered concentrations for each species displayed
302 different seasonal characteristics. The deweathered concentrations of some elements related with
303 industrial activities (e.g., Ga, Zn, and Cr) showed rapid decreases in autumn and winter compared
304 with other seasons during 2017-2020 (Figure 4), indicating that the optimization of the industrial
305 layout and shutdown of outdated industries were effective to decrease these element emissions
306 especially in the high-pollution season. Some elements derived from biomass burning including K
307 (66%) and Se (50%) also exhibited the most dramatic decreasing ratios in autumn. It was assumed
308 that enhanced crop residual burning occurred frequently during the autumn harvest season. Ke et al.
309 (2019) confirmed that the number of fire spots in October-November was even higher than that in
310 June and the burned area in the harvest season was highest during 2013-2017. However, the control
311 on open biomass burning has been implemented strictly in recent years, largely reducing the K and
312 Se emissions in autumn. It should be noted that the deweathered Pb (46%), Co (65%), and As (45%)
313 concentrations in winter did not display high decreasing ratios though the annual mean deweathered
314 Pb, Co and As levels experienced dramatic decreases. The result revealed that it was still difficult
315 to reduce the Pb, Co, and As emissions during the heating season because increased coal

316 consumption for domestic heating largely offset the contributions of emission control measures
317 (Zhu et al., 2018; Zhu et al., 2020).

318 Apart from the seasonal difference of each species, the decreasing ratios of these elements also
319 suffered from distinctly intra-weekly variations. The deweathered concentrations of most elements
320 except Ca, Cu, Ni, and V exhibited higher decreasing ratios at the weekends than on the weekdays
321 (Figure 5). Cui et al. (2020) have demonstrated that the weaker supervision on industrial enterprises
322 on weekends could lead to the higher concentrations of non-traffic elements such as K, As, Se, and
323 Cr in some cities. Fortunately, grid monitoring has been widely performed in Tangshan recently
324 (<http://hbepb.hebei.gov.cn/hbhjt/xwzx/jicengfengcai/101624062321621.html>), and many low-cost
325 sensors were installed at some energy-intensive industries, which could decrease the stealing
326 emissions of some elements. Nonetheless, the decreasing ratios of Ca, Cu, V, and Ni did not show
327 the regular intra-weekly characteristics. In recent years, Tangshan adopted strict traffic management
328 regulation and the nonlocal light duty vehicles were restricted to drive inside the urban area one day
329 per week based on the end number of the license plates (Westerdahl et al., 2009; Wu et al., 2011),
330 whereas the restrictions were not valid at weekends (Liu et al., 2007). Theoretically, the traffic
331 control should result in marked decreases of traffic-related element concentrations on weekdays
332 compared with weekends. However, in our study, some traffic-related elements such as Ca and Cu
333 did not show similar characteristics. Meanwhile, as the important tracer of vehicle emission, the
334 NO_x concentration in Tangshan did not show a regular intra-weekly pattern. It was supposed that
335 the vehicle volume in Tangshan has increased from 2.0 to 2.4 million (<http://tjj.hebei.gov.cn/>),
336 which largely offset the benefits of traffic controls. The shipping-related elements including V and
337 Ni also did not show regular intra-weekly variation because no heavy metal emission control
338 measures for shipping were performed.

339 3.3 The role of meteorology on the year-to-year variations of element concentrations

340 The difference between the original and the deweathered element concentrations could be
341 regarded as the concentrations contributed by meteorological parameters. The positive impacts of
342 meteorological parameters on the trace elements suggested that the meteorological conditions were
343 unfavorable to the pollutant diffusion, while the negative impacts of meteorological indicators
344 meant the favorable condition to trace elements. In our study, the roles of meteorological conditions

345 on Ca (-25%), V (-10%), Cr (-2.5%), Mn (-0.7%), Fe (-4.6%), Ni (-7.6%), and Cu (-21%) during
346 2017-2020 were negative (Figure S5), while the roles of meteorological parameters on other
347 elements were positive. The result suggested that those elements derived from vehicle emission (Ca,
348 Cu, and Fe), ferrous metal smelting (Cr and Mn), and heavy oil combustion (V and Ni) were less
349 sensitive to the emission reduction actions compared with other elements and the meteorological
350 conditions were much beneficial to the diffusion of these elements. In order to further reveal the key
351 meteorological factors for these elements, we used the RF model to calculate the variable
352 importance of all of these meteorological parameters including P, RH, T, WD, and WS. The result
353 suggested that Ca, Fe, and Cu were mainly influenced by T, whereas V, Ni, Cr, and Mn were often
354 associated with WD and WS (Figure 6). During the spring and summer in 2017-2020, the average
355 air temperature decreased from 8.9 and 27 to 7.2 and 26°C, respectively. The decreased air
356 temperature led to a higher water content in the soil and a lower tendency of dust suspension, and
357 might decrease the concentrations of Ca, Fe, and Cu (Manju et al., 2018; Yang et al., 2017; Lyu et
358 al., 2016). Although the annual average wind speed in Tangshan decreased from 1.70 to 1.45 m/s,
359 the mean wind speed from the southeastern direction displayed a slight increase from 1.34 to 1.50
360 m/s. Zhao et al. (2013) verified that V and Ni were usually emitted from heavy oil combustion of
361 ocean-going ship engines. Many coastal ports and ferrous metal smelting industries were located on
362 the southeastern direction of the sampling site, and thus the enhanced WS might promote the
363 dilution and dispersion of trace elements (Figures S6-S8). As shown in Figure S8, both ~~of~~V and Ni
364 showed ~~the~~ higher concentrations in the southeastern part of Tangshan and the concentrations
365 displayed gradual decreases along the Southeast-Northwest transect, which also demonstrated that
366 both of V and Ni in the sampling site could be derived from coastal shipping emission.

367 3.4 The impact of clean air policy on the source apportionment of the trace elements

368 Although the major sources of elements could be determined based on some important tracers
369 (e.g., K, V), the contributions of the major sources to each element still remained unknown.
370 Therefore, Positive matrix factorization (version PMF 5.0) was applied to identify more source
371 information of the elements in PM_{2.5} during 2017-2020 based on the deweathered levels. After 20
372 runs, more than 26000 samples were trained to determine the optimal six factors with the lowest
373 values of Q (robust) and Q (true). The BS, DISP, and BS-DISP methods confirmed that the most

374 reliable solution was obtained with six factors. The detailed information of the PMF analysis and
375 error diagnostics is summarized in Tables S4-S6.

376 As shown in Figure S9, the trace elements in PM_{2.5} during 2017-2020 showed similar
377 characteristics. Factor 1 possesses high loadings of K (55%) and Se (42%). K and Se were often
378 regarded as the major tracers of biomass burning. Due to the increasing usage of biomass fuels for
379 domestic heating during the heating season, K and Se in PM_{2.5} of Tangshan showed higher values
380 in winter, suggesting that these metals in fine particles could originate from the combustion of
381 biomass fuels. Except for the domestic heating, we found some episodes during the harvesting
382 season in late summer (2500 and 11.2 ng/m³) and early autumn (2600 and 9.5 ng/m³) also showed
383 extremely high concentrations of K, which might be linked with local biomass burning (Chen et al.,
384 2017). Based on the map of fire points and backward air masses trajectories (Figures S6-S8), the
385 metals released from biomass burning in the NCP could be transported to the sampling site by the
386 dominant southerly wind, which further proved the impacts of biomass burning (Chen et al., 2017).

387 The abundant elements in factor 2 included Ag (53%), Zn (51%), and Cu (36%). Owing to the
388 higher temperatures during the roasting, sintering and smelting processes for the extraction of Cu,
389 and Zn from ores, some metals such as Ag in nonferrous metal ores could be vaporized as a
390 byproduct and released into the flue gas (Pacyna and Pacyna, 2001; Wu et al., 2012). Therefore,
391 factor 2 was interpreted as the non-ferrous metal smelting source.

392 Factor 3 was characterized by a large mass fraction of Co (81%), Pb (61%), Hg (57%), and As
393 (39%). After the phase-out of leaded gasoline since 1980s, the contribution from coal combustion
394 to Pb showed rapid increase and accounted for the major fraction of particulate Pb (Das et al., 2018).
395 Meanwhile, Co and Hg were also treated as important byproducts released from coal burning and
396 the Co and Hg concentrations often increased significantly with the elevation of the burning
397 temperature (Tang et al., 2018). Tian et al. (2015) estimated that 73% of As, 56 % of Pb, and 47 %
398 of Hg were found to be emitted from coal combustion in China. Coal consumption in South China
399 was mainly driven by coal-fired power plants, while the coal-based heating was the major sector for
400 the coal consumption in the NCP. In our study, As, Co and Pb showed ~~the~~ higher concentrations in
401 winter (heating season) (18.7, 0.9, and 76 ng/m³) compared with other seasons (14, 0.6, and 51
402 ng/m³). The markedly seasonal discrepancies of As, Co and Pb strongly supported the impact of the

403 coal combustion for domestic heating on the enhancement of As, Co and Pb in the fine particles.

404 Factor 4 was distinguished by high loadings of Cr (78%) and Mn (39%), respectively. Cr and
405 Mn mainly originated from [the](#) metallurgical industry such as steel production and ferrous metal
406 smelting (Liu et al., 2018a; Tian et al., 2015; Zhu et al., 2018). China was responsible for more than
407 49% of the world steel production in 2017 (approximate 830 million tons), and 60% of the large
408 steel producers were located in China (Chang et al., 2018). Tangshan possesses many large steel
409 production industries such as Tangshan Steel, Qian'an Steel, and Guofeng Steel. Besides, some
410 industries of Capital Steel have been migrated into Tangshan (Li et al., 2019), which might increase
411 the Cr and Mn emissions.

412 Factor 5 explained 10.1% of the total species and it was characterized by high loadings of V
413 (88%) and Ni (51%). It was well documented that V was a key fingerprint of heavy oil combustion,
414 which was generally emitted from shipping emission and petrochemical refining (Shafer et al.,
415 2012). Ni was widely utilized as a tracer of fuel oil combustion in industries (Zhu et al., 2018).
416 Many oil-fired power plants were located in Tangshan for central heating (Yu et al., 2013). Based
417 on the backward trajectory and wind direction (Figures S6-S8), we found that high concentrations
418 of V and Ni might be derived from the southeastern air masses especially in summer and autumn,
419 indicating the impacts of coastal port and petroleum refinery industry. In addition, the V and Ni
420 concentrations displayed [the](#) gradual decreases along the Southeast-Northwest transect, indicating
421 the potential sources were located on Southeast Tangshan (Figure S8). Gathering evidence
422 suggested that the V/Ni ratio in petroleum coke with a low-sulfur content and fuel oil usage ranged
423 from 1 to 3 (Moreno et al., 2010). The annual mean ratios of V and Ni in our study reached 1.2
424 during the sampling period, which was in the range of this interval. The result also revealed that
425 petrochemical refining and heavy oil combustion derived from coastal shipping emission might be
426 an important source of V and Ni in the fine particles.

427 Factor 6 was characterized by high loadings of Ca (78%), Cu (32%), and Fe (33%), and moderate
428 loadings of Mn (31%) and Zn (29%). Some previous studies have demonstrated that Cu, Fe, and Zn
429 were released from tyre and brake wear because they were the necessary materials for brake pads
430 and the agents in brake linings (Dall'Osto et al., 2013; Hjortenkrans et al., 2007). Ca probably
431 originated from the road fugitive dust because it was one of the most abundant elements in the upper

432 soil (Alves et al., 2015; Liu et al., 2018a). Moreover, we have found that Fe, Ca, and Zn displayed
433 remarkably high values during the morning rush hours and a small peak during the sunset (Figure
434 S10), which was coincident to the diurnal variation of the traffic volume. Thus, the factor 6 was
435 identified as the traffic-related dust source.

436 Although six similar sources were revealed during 2017-2020, the contribution concentrations
437 and ratios of these sources varied greatly in these years. As shown in Figures 7 and 8, the
438 contribution concentrations of biomass burning, non-ferrous metal smelting, coal combustion, and
439 ferrous metal smelting to trace elements decreased from 1460, 480, 640, and 570 ng/m³ to 900, 230,
440 230, and 350 ng/m³, respectively. However, the contribution concentrations of heavy oil combustion
441 and traffic-related dust displayed a slight increase during 2017-2019, while they decreased rapidly
442 after 2019. The contribution concentrations for nearly all sources to the trace elements suffered
443 from showed decreases during 2017-2020 because the total deweathered levels of trace elements
444 experienced decreases in the past three years. However, the contribution ratios of these sources to
445 the trace elements did not show similar characteristics. For instance, the contribution ratio of the
446 traffic-related dust increased from 25% to 33%. In contrast, the contributions of non-ferrous metal
447 smelting and coal combustion decreased from 11% to 8% and 15% to 8%, respectively. The
448 contributions of ferrous metal smelting, heavy oil combustion, and biomass burning remained
449 relatively stable during this period.

450 Due to the strict implementation of the clean air policy, many outdated industrial capacities were
451 shut down and cleaner technologies have been upgraded were implemented, which facilitated the
452 production decreases of pig iron and coal-fired power plants (Ma et al., 2019). Hence, the
453 contribution concentrations and ratios of non-ferrous metal smelting and coal combustion
454 experienced dramatic decreases. Although the open biomass burning has been strictly restricted in
455 Tangshan (Chang et al., 2018), the contribution ratios of biomass burning to the trace elements in
456 PM_{2.5} remained relatively stable, which might be attributable to the rapid decreases of the
457 contributions derived from coal combustion and non-ferrous metal smelting. In addition, the biofuel
458 combustion was still widespread in some rural and suburb areas (Kamal et al., 2015; Li et al., 2020),
459 which might offset the decreases in the contributions of open biomass burning. Although the
460 contribution concentrations of traffic-related dust to trace elements also showed a slight decrease,

461 the contribution ratios of traffic-related dust to some trace elements exhibited marked increases (8%)
462 during 2017-2020 because the contribution ratios of metal smelting and coal combustion displayed
463 substantial decreases. The result also demonstrated that the implementation of coal to gas project
464 facilitated the decreases of trace element concentrations. In addition, the source variation trend also
465 suggested that the formulation of many new quality standards for non-road diesel fuels cannot fully
466 decrease the element emissions (Cui et al., 2017), and thus the control of traffic-related dust should
467 be enhanced in the future.

468 3.5 Health risk assessment of trace metals in PM_{2.5}

469 Although the trace metals only accounted for a minor fraction of the total mass concentration of
470 PM_{2.5}, it might pose a great threat to the human health because most of these metals were
471 bioavailable and non-degradable (Rai et al., 2019; Yi et al., 2011). Unfortunately, previous studies
472 mainly used filter sampling techniques to determine the concentrations of trace metals and then
473 assess their health risks (Cui et al., 2018; Huang et al., 2016). These low-resolution data might not
474 accurately reflect the real health risks triggered by metal exposure. In our study, we employed online
475 data to assess the health risks derived from metal exposure.

476 The health risks of trace metals could be classified into two types including carcinogenic and
477 non-carcinogenic risk. Based on the major parameters summarized in Tables S7 and S8, we
478 estimated both of the carcinogenic and non-carcinogenic risks of the major metals. To evaluate the
479 impacts of emission control measures on the element concentrations, both the health risks based on
480 the original element levels and the deweathered element concentrations were calculated. The mean
481 CR values based on the original concentrations were in the order of Pb (2.3×10^{-6} (adult) and 1.4×10^{-6}
482 (child)) > As (1.9×10^{-6} and 1.1×10^{-6}) > Cr (0.11×10^{-6} and 0.07×10^{-6}). The total CR values for adults
483 and children reached 4.3×10^{-6} and 2.6×10^{-6} (Table 2), respectively. The total CR values were located
484 in the range of the acceptable (10^{-6}) and least stringent risk levels (10^{-4}), which suggested that
485 Tangshan suffered from a slight metal carcinogenic risk. Among all of these metals, Pb and As
486 displayed the higher CR values. It was assumed that the coal combustion for domestic heating might
487 be the dominant factor for the higher risks of Pb and As in Tangshan because both Pb and As in
488 PM_{2.5} were mainly derived from coal combustion. With regard to the non-carcinogenic risks of the
489 trace metals, the HQ of As (1.2×10^{-2} and 2.9×10^{-2}) and Pb (6.8×10^{-4} and 17×10^{-4}) showed higher

490 values compared with other elements. The result indicated that nearly all elements did not display
491 potential non-carcinogenic risk because the HQ values of all the metals were less than 1. The total
492 HQ value of these metals was also lower than 1, indicating that the trace elements in Tangshan did
493 not show a significant non-carcinogenic risk.

494 By removing the impact of the meteorological conditions, we can isolate the impact of the clean
495 air policy on health risks associated with metal exposure alone. The decreased ratios of the CR
496 values based on the deweathered As and Pb concentrations during 2017-2020 were 54% and 62%,
497 respectively (Table 3). However, the decreased ratios of the CR values based on the original As and
498 Pb levels only reached 44%. The result suggested that the clean air policy in recent years
499 significantly decreased the As and Pb emissions. Additionally, the decreased ratios of the HQ values
500 for the original Cu (41%) and Zn (53%) were much less lower than those for the deweathered ones
501 (Cu: 47% and Zn: 59%). Nevertheless, some other elements did not show similar characteristics.
502 For instance, the decreased ratios of the HQ values for the original Cr (21%) and Fe (27%) were
503 even slightly higher than those for the deweathered ones (Cr: 19% and Fe: 23%). It was assumed
504 that the clean air policy in recent years facilitated the emission reduction of non-ferrous metal
505 smelting and coal combustion efficiently. However, the concentrations of the elements derived from
506 ferrous metal smelting and vehicle emission did not show marked decreases, which was in good
507 agreement with the source apportionment result in section 3.3. Thus, in the future work, it is highly
508 imperative to further reduce the industrial/traffic-related emissions in order to alleviate potential
509 health risks.

510 3.6 Limitations and uncertainties

511 It should be noted that our work is still subject to some limitations. At first, some elements such as
512 Cr (0.5) and Ga (0.5) showed relatively lower CV R² values though they were generally higher than
513 0.5. These elements might show the higher uncertainties during the meteorology-normalization
514 compared with other elements such as Cu (0.85) and K (0.85). Besides, few variables were applied
515 to deweather the element concentrations, which might be responsible for the lower CV R² value for
516 some elements. Due to the lack of available hourly emission inventory of each element, we only
517 used the time variable to train the model. This method still suffered from some uncertainties, which
518 should be improved by the establishment of near-time emission database.

519 **4. Conclusions and implications**

520 Three-year continuous hourly observation of elements in PM_{2.5} was conducted in Tangshan
521 during September 2017-August 2020. The effect of the clean air policy on the element
522 concentrations in PM_{2.5} was quantified. The main conclusions were ~~drawn~~ as follows:

523 (1) The deweathered concentrations of Ga, Co, Pb, Zn, and As showed rapid decreases from 1.52
524 to 0.42 ng/m³ (72%), 1.31 to 0.44 ng/m³ (67%), 92 to 35 ng/m³ (62%), 411 to 170 ng/m³ (59%),
525 and 21 to 10 ng/m³ (54%), respectively. The clean air actions played the important role on the
526 emission reduction of coal combustion and non-ferrous metal smelting.

527 (2) The deweathered levels of Ca (8.3%), Cr (19%), and Fe (23%) displayed relatively low
528 decreases compared with other elements, indicating that the vehicle emission and ferrous-
529 smelting industries might not be sensitive to the air clean policy.

530 (3) The deweathered levels of some elements related with industrial activities (e.g., Ga, Zn, and Cr)
531 exhibited rapid decreases in autumn and winter compared with other seasons during 2017-2020,
532 while the combustion-related elements such as Pb and As did not show high decreasing ratios
533 in winter. The enhanced coal consumption during the heating season offsets the benefits derived
534 from strict emission control measures.

535 (4) The favorable meteorological conditions promoted the decreases of Ca (-25%), V (-10%), Cr (-
536 2.6%), Mn (-0.68%), Fe (-4.6%), Ni (-7.6%), and Cu (-21%) concentrations.

537 (5) The contribution ratios of biomass burning, non-ferrous metal smelting, coal combustion,
538 ferrous metal smelting, heavy oil combustion, and traffic-related dust changed from 33%, 11%,
539 15%, 13%, 3%, and 25% to 33%, 8%, 8%, 13%, 4%, and 33%, respectively.

540 (6) All elements did not show significant noncarcinogenic and carcinogenic risks, while both As
541 and Pb still displayed relatively high health damages.

542 Our study presented detailed information about the impact of clean air policy on the chemical
543 compositions and source apportionment of trace elements in PM_{2.5} in Tangshan, and provided new
544 insights for the scientific community and policymakers. Many targeted measures could be
545 undertaken to alleviate the air pollution and further to reduce avoided premature health risks.
546 However, this study still suffered some limitations and more steps will be taken toward thoroughly
547 addressing these problems. First of all, the PMF model still showed some uncertainties, and thus

548 characterizing the isotopic signatures of the elements is of great significance. In addition, a Sunset
549 OC/EC analyzer, a Monitoring of Aerosols and Gases (MARGA) platform, and other on-line
550 measurements should be collocated to probe into the synergistic effect of emission reduction and
551 meteorology on air quality.

552 **Acknowledgements**

553 This work was supported by the National Natural Science Foundation of China (42107113).

554 **Data availability**

555 The boundary layer height dataset was obtained from the website of <https://www.ecmwf.int/>. The
556 dataset is archived in <https://zenodo.org/record/7031975#.Ywys8cjfmfU> (Li et al., 2022).

557 **Author contributions**

558 LR wrote the manuscript. LR, PM, ZWD, and HJM contributed to the conceptualization of the study.
559 LR, GYN, CYB, and PM conducted the research, and visualized the results. WGH revised the
560 manuscript.

561 **Competing interests**

562 The contact authors have declared that neither they nor their co-authors have any competing
563 interests.

564 **References**

- 565 Alies, B., Sasaki, I., Proux, O., Sayen, S., Guillon, E., Faller, P., and Hureau, C.: Zn impacts Cu
566 coordination to amyloid- β , the Alzheimer's peptide, but not the ROS production and the associated
567 cell toxicity, *Chem. Commun.*, 49, 1214-1216, 2013.
- 568 Alves, C. A., Gomes, J., Nunes, T., Duarte, M., Calvo, A. I., Custodio, D., Pio, C., Karanasiou, A., and
569 Querol, X.: Size-segregated particulate matter and gaseous emissions from motor vehicles in a road
570 tunnel, *Atmos. Res.*, 153, 134-144, <https://doi.org/10.1016/j.atmosres.2014.08.002>, 2015.
- 571 Ao, M., Qiu, G., Zhang, C., Xu, X., Zhao, L., Feng, X., Qin, S., and Meng, B.: Atmospheric deposition
572 of antimony in a typical mercury-antimony mining area, Shaanxi Province, Southwest China, *Environ.*
573 *Pollut.*, 245, 173-182, <https://doi.org/10.1016/j.envpol.2018.10.125>, 2019.
- 574 Chang, Y., Huang, K., Xie, M., Deng, C., Zou, Z., Liu, S., and Zhang, Y.: First long-term and near real-
575 time measurement of trace elements in China's urban atmosphere: temporal variability, source
576 apportionment and precipitation effect, *Atmos. Chem. Phys.*, 18, 11793-11812,
577 <https://doi.org/10.5194/acp-18-11793-2018>, 2018.
- 578 Chen, J., Li, C., Ristovski, Z., Milic, A., Gu, Y., Islam, M. S., Wang, S., Hao, J., Zhang, H., and He, C.:
579 A review of biomass burning: Emissions and impacts on air quality, health and climate in China, *Sci.*
580 *Total Environ.*, 579, 1000-1034, <https://doi.org/10.1016/j.scitotenv.2016.11.025>, 2017.
- 581 Chen, G. B., Li, S. S., Knibbs, L. D., Hamm, N. A. S., Cao, W., Li, T. T., Guo, J. P., Ren, H. Y., Abramson,
582 M. J., and Guo, Y. M.: A machine learning method to estimate PM_{2.5} concentrations across China with
583 remote sensing, meteorological and land use information, *Sci. Total Environ.*, 636, 52-60,
584 <https://doi.org/10.1016/j.scitotenv.2018.04.251>, 2018.
- 585 Clements, A. L., Buzcuguvan, B., Fraser, M. P., Kulkarni, P., and Chellam, S.: Role of particulate metals
586 in heterogenous secondary sulfate formation, *Atmos. Environ.*, 75, 233-240,
587 <https://doi.org/10.1016/j.atmosenv.2013.04.038>, 2013.
- 588 Clements, N., Eav, J., Xie, M., Hannigan, M. P., Miller, S. L., Navidi, W., Peel, J. L., Schauer, J. J., Shafer,
589 M. M., and Milford, J. B.: Concentrations and source insights for traceelements infine and coarse
590 particulate matter, *Atmos. Environ.*, 89, 373-381, <https://doi.org/10.1016/j.atmosenv.2014.01.011>,
591 2014.
- 592 Cui, L., Duo, B., Zhang, F., Li, C., Fu, H., and Chen, J.: Physiochemical characteristics of aerosol
593 particles collected from the Jokhang Temple indoors and the implication to human exposure, *Environ.*
594 *Pollut.*, 236, 992-1003, <https://doi.org/10.1016/j.envpol.2017.10.107>, 2018.
- 595 Cui, M., Chen, Y., Feng, Y., Li, C., Zheng, J., Tian, C., Yan, C., and Zheng, M.: Measurement of PM and
596 its chemical composition in real-world emissions from non-road and on-road diesel vehicles, *Atmos.*
597 *Chem. Phys.*, 17, 6779-6795, <https://doi.org/10.5194/acp-17-6779-2017>, 2017.
- 598 Cui, X., Wang, X., and Liu, B.: The characteristics of heavy metal pollution in surface dust in Tangshan,
599 a heavily industrialized city in North China, and an assessment of associated health risks, *J. Geochem.*
600 *Explor.*, 210, 106432, 2020.
- 601 Cui, Y., Ji, D., Chen, H., Gao, M., Maenhaut, W., He, J., and Wang, Y.: Characteristics and sources of
602 hourly trace elements in airborne fine particles in urban Beijing, China, *J. Geophys. Res. Atmos.*, 124,
603 11595-11613, <https://doi.org/10.1029/2019JD030881>, 2019.
- 604 D'Alessandro, A., Lucarelli, F., Mandò, P. A., Marcazzan, G., Nava, S., Prati, P., Valli, G., Vecchi, R.,
605 Zucchiatti, A.: Hourly elemental composition and sources identification of fine and coarse PM₁₀
606 particulate matter in four Italian towns, *J. Aerosol Sci.*, 34, 243-259, 2003.

607 Dall'Osto, M., Querol, X., Amato, F., Karanasiou, A., Lucarelli, F., Nava, S., Calzolari, G., and Chiari,
608 M.: Hourly elemental concentrations in PM_{2.5} aerosols sampled simultaneously at urban background
609 and road site during SAPUSS - diurnal variations and PMF receptor modelling, *Atmos. Chem. Phys.*,
610 13, 4375-4392, 2013.

611 Das, R., Mohtar, A. T. B. M., Rakshit, D., Shome, D., and Wang, X.: Sources of atmospheric lead (Pb)
612 in and around an Indian megacity, *Atmos. Environ.*, 193, 57-65,
613 <https://doi.org/10.1016/j.atmosenv.2018.08.062>, 2018.

614 Duan, J. and Tan, J.: Atmospheric heavy metals and arsenic in China: situation, sources and control
615 policies, *Atmos. Environ.*, 74, 93-101, 10.1016/j.atmosenv.2013.03.031, 2013.

616 Fang, B., Zhang, L., Zeng, H., Liu, J., Yang, Z., Wang, H., Wang, Q., and Wang, M.: PM_{2.5}-bound
617 polycyclic aromatic hydrocarbons: sources and health risk during non-heating and heating periods
618 (Tangshan, China), *Int. J. Environ. Res. Public Health* 17, 483, 2020.

619 Fernandez, J. A., Rey, A., and Carballeira, A.: An extended study of heavy metal deposition in Galicia
620 (NW Spain) based on moss analysis, *Sci. Total Environ.*, 254, 31-44, 10.1016/S0048-9697(00)00431-
621 9, 2000.

622 Furger, M., Minguillon, M. C., Yadav, V., Slowik, J.G., Hüglin, C., Fröhlich, R., Petterson, K.,
623 Baltensperger, U., and Prevot, A. S. H.: Elemental composition of ambient aerosols measured with
624 high temporal resolution using an online XRF spectrometer, *Atmos. Meas. Tech.*, 10, 2061-2076,
625 <https://doi.org/10.5194/amt-10-2061-2017>, 2017.

626 Geng, G., Xiao, Q., Zheng, Y., Tong, D., Zhang, Y., Zhang, X., Zhang, Q., He, K., and Liu, Y.: Impact of
627 China's air pollution prevention and control action plan on PM_{2.5} chemical composition over eastern
628 China, *Sci. China Earth Sci.*, 62, 1872-1884, <https://doi.org/10.1007/s11430-018-9353-x>, 2019.

629 Grivas, G., Cheristanidis, S., Chaloulakou, A., Koutrakis, P., & Mihalopoulos, N.: Elemental composition
630 and source apportionment of fine and coarse particles at traffic and urban background locations in
631 Athens, Greece, *Aerosol Air Qual. Res.*, 18, 1642-1659, 2018.

632 Guo, J., Tilgner, A., Yeung, C., Wang, Z., Louie, P. K. K., Luk, C. W. Y., Xu, Z., Yuan, C., Gao, Y., and
633 Poon, S.: Atmospheric peroxides in a polluted subtropical environment: seasonal variation, sources
634 and sinks, and importance of heterogeneous processes, *Environ. Sci. Technol.*, 48, 1443-1450,
635 <https://doi.org/10.1021/es403229x>, 2014.

636 Harmens, H., Norris, D. A., Steinnes, E., Kubin, E., Piispanen, J., Alber, R., Aleksiyenak, Y., Blum, O.,
637 Coskun, M., and Dam, M.: Mosses as biomonitors of atmospheric heavy metal deposition: Spatial
638 patterns and temporal trends in Europe, *Environ. Pollut.*, 158, 3144-3156,
639 <https://doi.org/10.1016/j.envpol.2010.06.039>, 2010.

640 He, Q., Zhang, M., Song, Y., and Huang, B.: Spatiotemporal assessment of PM_{2.5} concentrations and
641 exposure in China from 2013 to 2017 using satellite-derived data, *J. Cleaner Prod.*, 286, 124965,
642 <https://doi.org/10.1016/j.jclepro.2020.124965>, 2021.

643 Hjortenkrans, D. S., Bergbäck, B. G., and Häggerud, A. V.: Metal emissions from brake linings and tires:
644 case studies of Stockholm, Sweden 1995/1998 and 2005, *Environ. Sci. Technol.*, 41, 5224-5230,
645 <https://doi.org/10.1021/es070198o>, 2007.

646 Holden, P. A., Gardeatorresdey, J. L., Klaessig, F., Turco, R. F., Mortimer, M., Hundrinke, K., Hubal, E.
647 A. C., Avery, D., Barcelo, D., and Behra, R.: Considerations of environmentally relevant test
648 conditions for improved evaluation of ecological hazards of engineered nanomaterials, *Environ. Sci.*
649 *Technol.*, 50, 6124-6145, <https://doi.org/10.1021/acs.est.6b00608>, 2016.

650 Huang, C., Bao, L., Luo, P., Wang, Z., Li, S., and Zeng, E. Y.: Potential health risk for residents around

651 a typical e-waste recycling zone via inhalation of size-fractionated particle-bound heavy metals, J.
652 Hazard. Mater., 317, 449-456, 10.1016/j.jhazmat.2016.05.081, 2016.

653 Jeong, C., Wang, J. M., and Evans, G. J.: Source apportionment of urban particulate matter using hourly
654 resolved trace metals, organics, and inorganic aerosol components, Atmos. Chem. Phys., 1-32,
655 <https://doi.org/10.5194/acp-2016-189>, 2016.

656 Kamal, A., Cincinelli, A., Martellini, T., and Malik, R. N.: A review of PAH exposure from the
657 combustion of biomass fuel and their less surveyed effect on the blood parameters, Environ. Sci. Pollut.
658 Res., 22, 4076-4098, 10.1007/s11356-014-3748-0, 2015.

659 Kang, S., Chen, P., Li, C., Liu, B., and Cong, Z.: Atmospheric aerosol elements over the inland Tibetan
660 Plateau: concentration, seasonality, and transport, Aerosol Air Qual. Res., 16, 789-800, 2016.

661 Ke, H. B., Gong, S. L., He, J. J., Zhou, C. H., Zhang, L., Zhou, Y. K.: Spatial and temporal distribution
662 of open bio-mass burning in China from 2013 to 2017, Atmos. Environ., 210, 156-165, 2019.

663 Li, R., Fu, H., Cui, L., Li, J., Wu, Y., Meng, Y., Wang, Y., and Chen, J.: The spatiotemporal variation and
664 key factors of SO₂ in 336 cities across China, J. Cleaner Prod., 210, 602-611,
665 <https://doi.org/10.1016/j.jclepro.2018.11.062>, 2019.

666 Li, R., Guo, J. P., Geng, G. N., Xiao, Q. Y., and Zhang, Q.: Satellite-derived long-term estimates of full-
667 coverage PM₁ concentrations across China based on a stacking decision tree model, Atmos. Environ.,
668 255, 118448, 2021a.

669 Li, R., Zhao, Y., Fu, H., Chen, J., Peng, M., and Wang, C.: Substantial changes in gaseous pollutants and
670 chemical compositions in fine particles in the North China Plain during the COVID-19 lockdown
671 period: anthropogenic vs. meteorological influences, Atmos. Chem. Phys., 21, 8677-8692,
672 <https://doi.org/10.5194/acp-21-8677-2021>, 2021b.

673 Li, R., Peng, M., Zhao, W. D., Wang, G. H., and Hao, J. M.: Data for “Measurement Report: Rapid
674 changes of chemical characteristics and health risks for high time-resolved trace elements in PM_{2.5} in
675 a typical industrial city in response to stringent clean air actions”, [dataset],
676 <https://zenodo.org/record/7031975#.Ywys8cjfmfU>, 2022.

677 Li, Z., Jiang, J., Ma, Z., Fajardo, O. A., Deng, J., and Duan, L.: Influence of flue gas desulfurization
678 (FGD) installations on emission characteristics of PM_{2.5} from coal-fired power plants equipped with
679 selective catalytic reduction (SCR), Environ. Pollut., 230, 655-662,
680 <https://doi.org/10.1016/j.envpol.2017.06.103>, 2017.

681 Li, Z., Wang, Y., Li, Z., Guo, S., and Hu, Y.: Levels and sources of PM_{2.5}-associated pahs during and after
682 the wheat harvest in a central rural area of the beijing-tianjin-hebei (bth) region, Aerosol Air Qual.
683 Res., 20, 1070-1082, 2020.

684 Lin, Y., Hsu, S., Chou, C. C. K., Zhang, R., Wu, Y., Kao, S., Luo, L., Huang, C., Lin, S., and Huang, Y.:
685 Wintertime haze deterioration in Beijing by industrial pollution deduced from trace metal fingerprints
686 and enhanced health risk by heavy metals, Environ. Pollut., 208, 284-293,
687 <https://doi.org/10.1016/j.envpol.2015.07.044>, 2016.

688 Liu, H., He, K., Wang, Q., Huo, H., Lents, J., Davis, N., Nikkila, N., Chen, C., Osses, M., and He, C.:
689 Comparison of vehicle activity and emission inventory between Beijing and Shanghai, J. Air Waste
690 Manage., 57, 1172-1177, <https://doi.org/10.3155/1047-3289.57.10.1172>, 2007.

691 Liu, J., Chen, Y., Chao, S., Cao, H., Zhang, A., and Yang, Y.: Emission control priority of PM_{2.5}-bound
692 heavy metals in different seasons: A comprehensive analysis from health risk perspective, Sci. Total
693 Environ., 644, 20-30, <https://doi.org/10.1016/j.scitotenv.2018.06.226>, 2018a.

694 Liu, R., Men, C., Yu, W., Xu, F., Wang, Q., and Shen, Z.: Uncertainty in positive matrix factorization

695 solutions for PAHs in surface sediments of the Yangtze River Estuary in different seasons,
696 Chemosphere, 191, 922-936, <https://doi.org/10.1016/j.chemosphere.2017.10.070>, 2018b.

697 Lopez-Cruz, J., Crespo-Salvador, O., Fernandez-Crespo, E., Garcia-Agustin, P., and Gonzalez-Bosch, C.:
698 Absence of Cu-Zn superoxide dismutase BCSOD1 reduces Botrytis cinerea virulence in Arabidopsis
699 and tomato plants, revealing interplay among reactive oxygen species, callose and signaling pathways,
700 Mol. Plant Pathol., 18, 16-31, 2016.

701 Lyu, X. P., Chen, N., Guo, H., Zeng, L. W., Zhang, W. H., Shen, F., Quan, J. H., Wang, N.: Chemical
702 characteristics and causes of airborne particulate pollution in warm seasons in Wuhan, central China,
703 Atmos. Chem. Phys., 16, 10671-10687, www.atmos-chem-phys.net/16/10671/2016/, 2016

704 Lyu, Y., Zhang, K., Chai, F., Cheng, T., Yang, Q., Zheng, Z., and Li, X.: Atmospheric size-resolved trace
705 elements in a city affected by non-ferrous metal smelting: Indications of respiratory deposition and
706 health risk, Environ. Pollut., 224, 559-571, <https://doi.org/10.1016/j.envpol.2017.02.039>, 2017.

707 Ma, Z., Liu, R., Liu, Y., and Bi, J.: Effects of air pollution control policies on PM_{2.5} pollution
708 improvement in China from 2005 to 2017: a satellite-based perspective, Atmos. Chem. Phys., 19,
709 6861-6877, <https://doi.org/10.5194/acp-19-6861-2019>, 2019.

710 Manju, A., Kalaiselvi, K., Dhananjayan, V., Palanivel, M., Banupriya, G., Vidhya, M., Panjakumar, K.,
711 and Ravichandran, B.: Spatio-seasonal variation in ambient air pollutants and influence of
712 meteorological factors in Coimbatore, Southern India, Air Qual. Atmos. Health 11, 1179-1189,
713 <https://doi.org/10.1007/s11869-018-0617-x>, 2018.

714 Manousakas, M., Papaefthymiou, H., Diapouli, E., Migliori, A., Karydas, A. G., Bogdanovic-Radovic,
715 I., and Eleftheriadis, K.: Assessment of PM_{2.5} sources and their corresponding level of uncertainty in
716 a coastal urban area using EPA PMF 5.0 enhanced diagnostics, Sci. Total Environ., 574, 155-164, 2017.

717 Micheline, G., Rachida, C., Celine, M., Gaby, K., Rachid, A., and Petru, J.: Levels of Pb, Cd, Hg and As
718 in fishery products from the eastern Mediterranean and human health risk assessment due to their
719 Consumption, Intern. J. Environ. Res., 13, 443-455, <https://doi.org/10.1007/s41742-019-00185-w>,
720 2019.

721 Moreno, T., Querol, X., Alastuey, A., La Rosa, J. D. D., La Campa, A. M. S. D., Minguillon, M., Pandolfi,
722 M., Gonzalez-Castanedo, Y., Monfort, E., and Gibbons, W.: Variations in vanadium, nickel and
723 lanthanoid element concentrations in urban air, Sci. Total Environ., 408, 4569-4579,
724 <https://doi.org/10.1016/j.scitotenv.2010.06.016>, 2010.

725 Norris, G., Duvall, R., Brown, S., and Bai, S.: EPA positive matrix factorization (PMF) 5.0 fundamentals
726 and user guide. U.S. Environmental Protection Agency Office of Research and Development,
727 Washington, DC, 20460, (i-124, EPA/600/R-14/108, April), 2014.

728 Oldani, K. M., Mladenov, N., Williams, M., Campbell, C. M., and Lipson, D. A.: Seasonal patterns of
729 dry deposition at a high-elevation site in the colorado rocky mountains, J. Geophys. Res. Atmos., 122,
730 11183-11200, 2017.

731 Olujimi, O. O., Oputu, O., Fatoki, O. S., Opatoyinbo, O. E., Aroyewun, O. A., and Baruani, J.: Heavy
732 metals speciation and human health risk assessment at an illegal gold mining site in Igun, Osun State,
733 Nigeria, J. Health. Pollut., 5, 19-32, 2015.

734 Paatero, P. and Tapper, U.: Positive matrix factorization: A non-negative factor model with optimal
735 utilization of error estimates of data values, Environmetrics, 5, 111-126, 1994.

736 Pacyna, J. M. and Pacyna, E. G.: An assessment of global and regional emissions of trace metals to the
737 atmosphere from anthropogenic sources worldwide, Environ. Rev., 9, 269-298, 2001.

738 Prati, P., Zucchiatti, A., Lucarelli, F., Mandò, P. A.: Source apportionment near a steel plant in Genoa

739 (Italy) by continuous aerosol sampling and PIXE analysis, *Atmos. Environ.*, 34, 3149-3157, 2000.

740 Rai, P. K., Lee, S. S., Zhang, M., Tsang, Y. F., and Kim, K.: Heavy metals in food crops: Health risks,
741 fate, mechanisms, and management, *Environ. Int.*, 125, 365-385, 2019.

742 Rasmussen, P. E.: Long-range atmospheric transport of trace metals: the need for geoscience perspectives,
743 *Environ. Earth Sci.*, 33, 96-108, 1998.

744 Reff, A., Eberly, S. I., and Bhave, P. V.: Receptor modeling of ambient particulate matter data using
745 positive matrix factorization: review of existing methods, *J. Air Waste Manage.*, 57, 146-154, 2007.

746 Ren, Z., Zhang, B., Lu, P., Li, C., Gao, L., and Zheng, M.: Characteristics of air pollution by
747 polychlorinated dibenzo-p-dioxins and dibenzofurans in the typical industrial areas of Tangshan City,
748 China, *J. Environ. Sci. -China*, 23, 228-235, 2011.

749 Saffari, A., Daher, N., Shafer, M. M., Schauer, J. J., and Sioutas, C.: Global perspective on the oxidative
750 potential of airborne particulate matter: a synthesis of research findings, *Environ. Sci. Technol.*, 48,
751 7576-7583, 2014.

752 Shafer, M. M., Toner, B. M., Overdier, J. T., Schauer, J. J., Fakra, S. C., Hu, S., Herner, J.D., and Ayala,
753 A.: Chemical speciation of vanadium in particulate matter emitted from diesel vehicles and urban
754 atmospheric aerosols, *Environ. Sci. Technol.*, 46, 189-195, 2012.

755 Shi, G., Teng, J., Ma, H., Li, Y., and Sun, B.: Metals and metalloids in precipitation collected during
756 CHINARE campaign from Shanghai, China, to Zhongshan Station, Antarctica: Spatial variability and
757 source identification, *Global Biogeochem. Cyc.*, 29, 760-774, 2015.

758 Song, Z. F.: An assessment of the heavy metal pollution and potential ecological hazards in urban soil of
759 Tangshan City, *Geology in China*, 38, 1379-1386, 2011.

760 Storelli, M. M.: Potential human health risks from metals (Hg, Cd, and Pb) and polychlorinated biphenyls
761 (PCBs) via seafood consumption : estimation of target hazard quotients (THQs) and toxic equivalents
762 (TEQs), *Food Chem. Toxicol.*, 46, 2782-2788, 2008.

763 Taghvaei, S., Sowlat, M. H., Mousavi, A., Hassanvand, M. S., Yunesian, M., Naddafi, K., and Sioutas,
764 C.: Source apportionment of ambient PM_{2.5} in two locations in central Tehran using the Positive Matrix
765 Factorization (PMF) model, *Sci. Total Environ.*, 628-629, 672-686, 2018.

766 Tang, Q., Sheng, W., Li, L., Zheng, L., Miao, C., and Sun, R.: Alteration behavior of mineral structure
767 and hazardous elements during combustion of coal from a power plant at Huainan, Anhui, China,
768 *Environ. Pollut.*, 239, 768-776, 2018.

769 Tian, H., Zhu, C., Gao, J., Cheng, K., Hao, J., Wang, K., Hua, S., Wang, Y., and Zhou, J.: Quantitative
770 assessment of atmospheric emissions of toxic heavy metals from anthropogenic sources in China:
771 historical trend, spatial distribution, uncertainties, and control policies, *Atmos. Chem. Phys.*, 15,
772 10127-10147, 2015.

773 Tianxue, W., Yuesi, W., Shihyu, C., and Guangren, L.: On-line measurement of water-soluble ions in
774 ambient particles, *Adv. Atmos. Sci.*, 23, 586-592, 2006.

775 Wang, S., Su, H., Chen, C., Tao, W., Streets, D. G., Lu, Z., Zheng, B., Carmichael, G. R., Lelieveld, J.,
776 and Pöschl, U.: Natural gas shortages during the “coal-to-gas” transition in China have caused a large
777 redistribution of air pollution in winter 2017, *P. Natl. Acad. Sci. USA*, 117, 31018-31025, 2020a.

778 Wang, S., Su, H., Chen, C., Tao, W., Streets, D. G., Lu, Z., Zheng, B., Carmichael, G. R., Lelieveld, J.,
779 Pöschl, U., and Cheng, Y.: Natural gas shortages during the “coal-to-gas” transition in China have
780 caused a large redistribution of air pollution in winter 2017, *P. Natl. Acad. Sci. USA*, 117, 31018-
781 31025, 2020b.

782 Westerdahl, D., Wang, X., Pan, X., and Zhang, K. M.: Characterization of on-road vehicle emission

783 factors and microenvironmental air quality in Beijing, China, *Atmos. Environ.*, 43, 697-705,
784 <https://doi.org/10.1016/j.atmosenv.2008.09.042>, 2009.

785 Witt, M. L. I., Baker, A. R., and Jickells, T. D.: Atmospheric trace metals over the Atlantic and South
786 Indian Oceans: Investigation of metal concentrations and lead isotope ratios in coastal and remote
787 marine aerosols, *Atmos. Environ.*, 40, 5435-5451, <https://doi.org/10.1016/j.atmosenv.2006.04.041>,
788 2006.

789 Wu, Q., Wang, S., Zhang, L., Song, J., Yang, H., and Meng, Y.: Update of mercury emissions from China's
790 primary zinc, lead and copper smelters, 2000-2010, *Atmos. Chem. Phys.*, 12, 18207-18242,
791 <https://doi.org/10.5194/acp-12-11153-2012>, 2012.

792 Wu, Y., Wang, R., Zhou, Y., Lin, B., Fu, L., He, K., and Hao, J.: On-road vehicle emission control in
793 beijing: past, present, and future, *Environ. Sci. Technol.*, 45, 147-153,
794 <https://doi.org/10.1021/es1014289>, 2011.

795 Xiao, Q., Geng, G., Liang, F., Wang, X., Lv, Z., Lei, Y., Huang, X., Zhang, Q., Liu, Y., and He, K.:
796 Changes in spatial patterns of PM_{2.5} pollution in China 2000-2018: Impact of clean air policies,
797 *Environ. Int.*, 141, 105776, <https://doi.org/10.1016/j.envint.2020.105776>, 2020.

798 Yang, Q., Yuan, Q., Li, T., Shen, H., and Zhang, L.: The relationships between PM_{2.5} and meteorological
799 factors in China: seasonal and regional variations, *Int. J. Environ. Res. Public Health* 14, 1510, 2017.

800 Yi, Y., Yang, Z., and Zhang, S.: Ecological risk assessment of heavy metals in sediment and human health
801 risk assessment of heavy metals in fishes in the middle and lower reaches of the Yangtze River basin,
802 *Environ. Pollut.*, 159, 2575-2585, <https://doi.org/10.1016/j.envpol.2011.06.011>, 2011.

803 Yu, L., Wang, G., Zhang, R., Zhang, L., Song, Y., Wu, B., Li, X., An, K., and Chu, J.: Characterization
804 and source apportionment of pm_{2.5} in an urban environment in Beijing, *Aerosol Air Qual. Res.*, 13,
805 574-583, doi: 10.4209/aaqr.2012.07.0192, 2013.

806 Zhang, J., Zhou, X., Wang, Z., Yang, L., Wang, J., Wang, W.: Trace elements in PM_{2.5} in Shandong
807 Province: Source identification and health risk assessment, *Sci. Total Environ.*, 621, 558-577, 2018.

808 Zhang, Q., Zheng, Y., Tong, D., Shao, M., Wang, S., Zhang, Y., Xu, X., Wang, J., He, H., Liu, W., Ding,
809 Y., Lei, Y., Li, J., Wang, Z., Zhang, X., Wang, Y., Cheng, J., Liu, Y., Shi, Q., Yan, L., Geng, G., Hong,
810 C., Li, M., Liu, F., Zheng, B., Cao, J., Ding, A., Gao, J., Fu, Q., Huo, J., Liu, B., Liu, Z., Yang, F., He,
811 K., and Hao, J.: Drivers of improved PM_{2.5} air quality in China from 2013 to 2017, *P. Natl. Acad. Sci.*
812 *USA*, 116, 24463-24469, <https://doi.org/10.1073/pnas.1907956116>, 2019.

813 Zhao, M., Zhang, Y., Ma, W., Fu, Q., Yang, X., Li, C., Zhou, B., Yu, Q., and Chen, L.: Characteristics
814 and ship traffic source identification of air pollutants in China's largest port, *Atmos. Environ.*, 64, 277-
815 286, <https://doi.org/10.1016/j.atmosenv.2012.10.007>, 2013.

816 Zhu, C., Tian, H., Hao, Y., Gao, J., Hao, J., Wang, Y., Hua, S., Wang, K., and Liu, H.: A high-resolution
817 emission inventory of anthropogenic trace elements in Beijing-Tianjin-Hebei (BTH) region of China,
818 *Atmos. Environ.*, 191, 452-462, <https://doi.org/10.1016/j.atmosenv.2018.08.035>, 2018.

819 Zhu, C., Tian, H., and Hao, J.: Global anthropogenic atmospheric emission inventory of twelve typical
820 hazardous trace elements, 1995-2012, *Atmos. Environ.*, 220, 117061,
821 <https://doi.org/10.1016/j.atmosenv.2019.117061>, 2020.

822

Figure 1 Topographic map of China indicating the location of Tangshan (a), the sampling site (b), and some major industrial points (b). The population distribution of Tangshan is also depicted in (b).

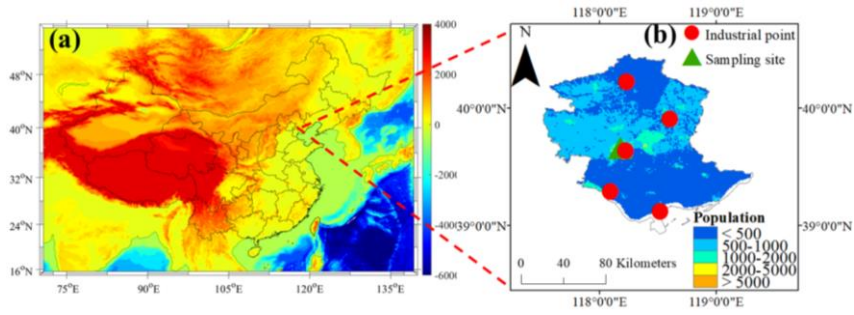


Figure 2 Bar chart of the concentrations of 16 trace elements including K, Fe, Ca, Zn, Pb, Mn, Fe, As, Se, V, Cr, Ag, Ni, Hg, Ga, and Co. The bars and black lines represent mean values and associated standard deviations, respectively.

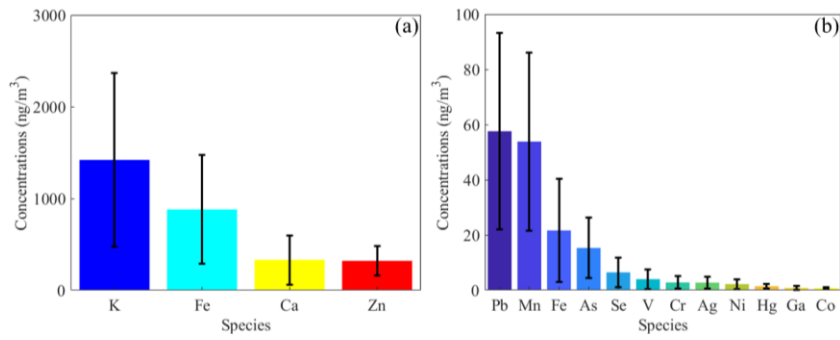


Figure 3 Inter-annual variations of the original (red) and deweathered (manganese purple) element concentrations (ng/m^3) in $\text{PM}_{2.5}$ in Tangshan. The dark, nattier blue, and nattier yellow backgrounds represent the species during 2017-2018 (from September in 2017 to August in 2018), 2018-2019 (from September in 2018 to August in 2019), and 2019-2020 (from September in 2019 to August in 2020). The bars and black lines represent mean values and associated standard deviations, respectively.

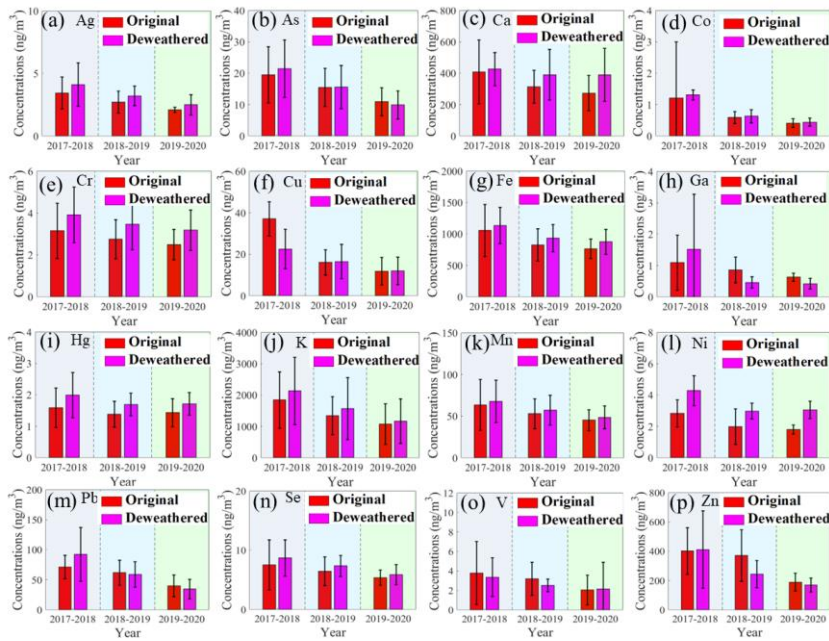


Figure 4 Original (red and orange) and deweathered (green and blue) element concentrations (ng/m^3) in $\text{PM}_{2.5}$ in Tangshan in four seasons during 2017-2018, 2018-2019, and 2019-2020. S1, U1, A1, and W1 represent the spring, summer, autumn, and winter during 2017-2018. S2, U2, A2, and W2 denote the spring, summer, autumn, and winter during 2018-2019. S3, U3, A3, and W3 are the spring, summer, autumn, and winter during 2019-2020. The points and shaded areas represent mean values and associated standard deviations, respectively.

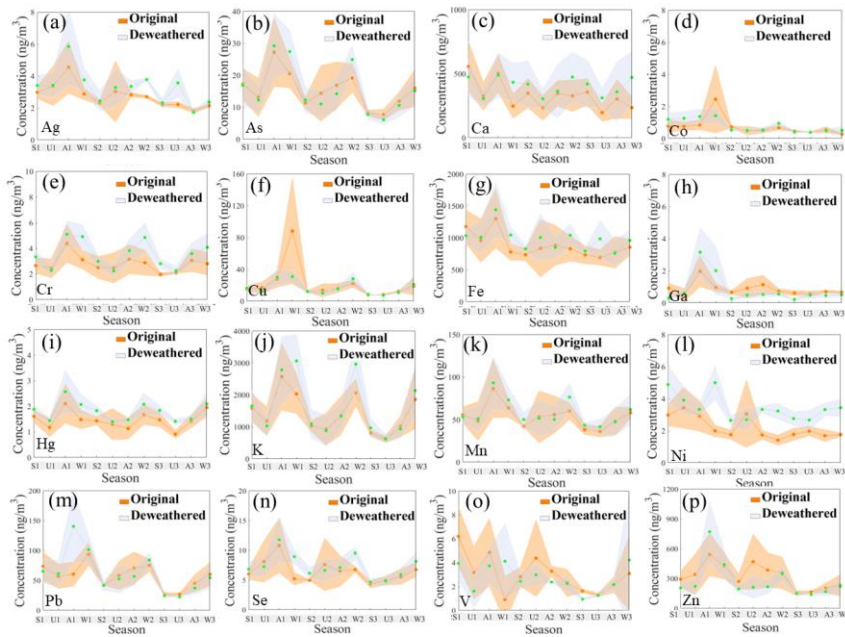


Figure 5 Weekly variations of the original (green) and deweathered (orange) element concentrations (ng/m^3) in $\text{PM}_{2.5}$ in Tangshan. The green and dark backgrounds denote the error bars of the original and deweathered elements, respectively. The bars and black lines represent mean values and associated standard deviations, respectively.

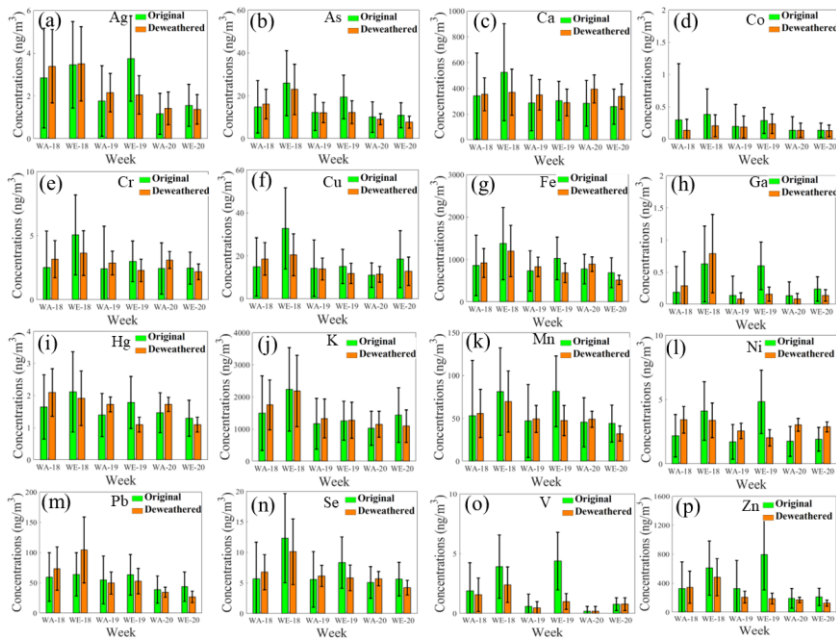


Figure 6 Relative importance of the predictors for the prediction of trace elements. The columns in the figure represent the variable importance in the RF models for the trace elements. P, RH, T, WD, WS, DOW, HOY, DOY, and Year denote air pressure, relative humidity, air temperature, wind direction, wind speed, day of week, hour of day, day of year, and study year, respectively.

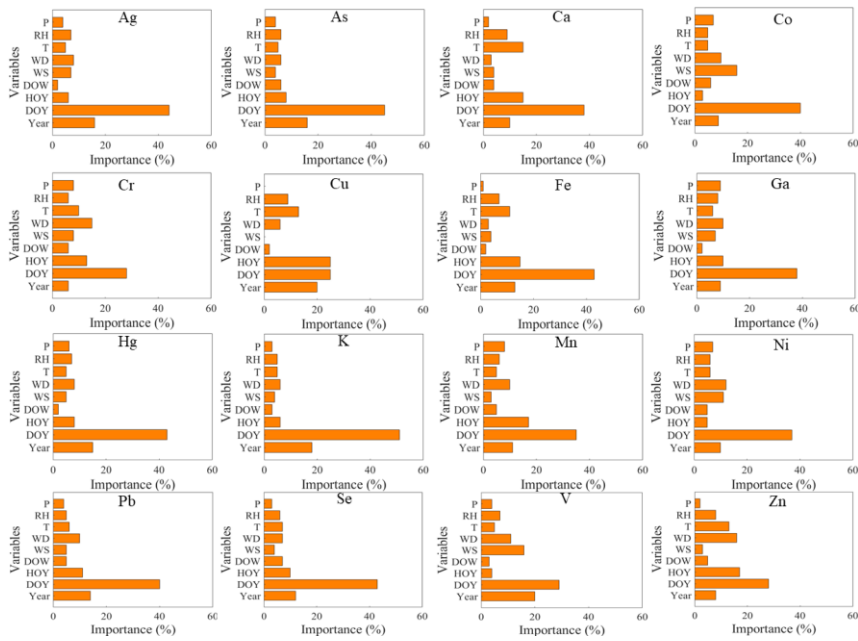


Figure 7 Deweathered mean concentrations of trace elements derived from six sources in Tangshan during 2017-2020.

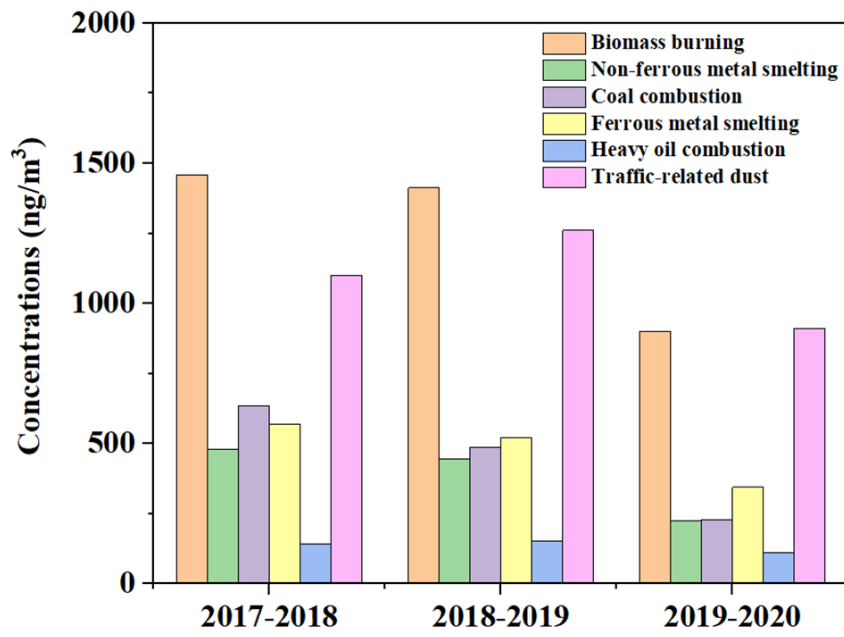


Figure 8 Average contributions of the six sources to the deweathered concentrations of the elements in PM_{2.5} based on the PMF model. The red panel means the biomass burning; the green panel denotes the non-ferrous metal smelting; the blue one represents the coal combustion; the cyan one is the ferrous metal smelting; the pink one represents the heavy oil combustion; and the yellow one denotes the traffic-related dust. (a), (b), and (c) represent the source contributions during 2017-2018, 2018-2019, and 2019-2020, respectively.

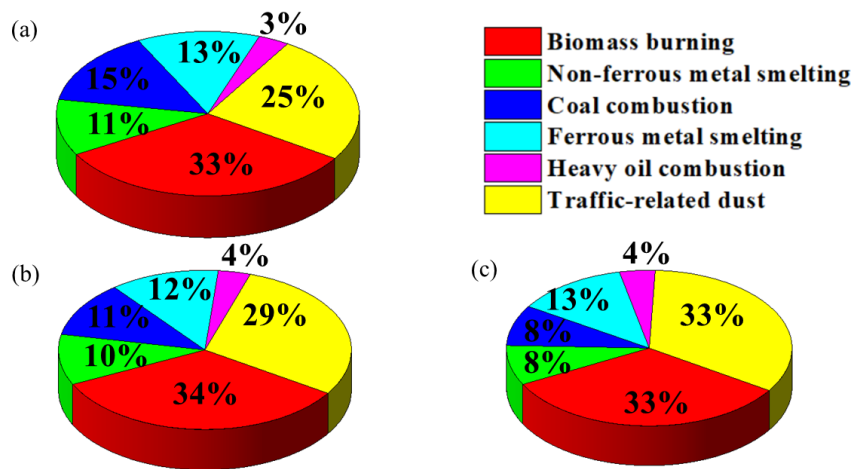


Table 1 Comparison of the element concentrations in PM_{2.5} of Tangshan and the standard values for these elements in World Health Organization (WHO), China, Europe, and the United States (Unit: ng/m³).

Elements	Mean±SD	CAAQS	WHO	EU	United States
Co	0.7±0.2				
Ga	0.9±0.7				
Hg	1.47±0.8	50	1000		
Ni	2.2±1.8		25	20	
Ag	2.8±2.1				
Cr	2.8±2.2	0.03	0.3		
V	4.0±3.6				
Se	6.5±5.3				
As	15.3±11.0	6	6.6	6	
Cu	22±19				
Mn	54±32				
Pb	58±36		1000		150
Zn	320±160				
Ca	330±270				
Fe	880 ± 590				
K	1420±950				

Table 2 Non-carcinogenic and carcinogenic risks for the original element levels in PM_{2.5}.

Age	Year	Indicator	Cr	Mn	Fe	Co	Ni	Cu	Zn	As	Pb	
Adult	2017-2018	HQ	2.5×10^{-3}	1.07×10^{-4}	3.6×10^{-4}	4.5×10^{-3}	0.3×10^{-4}	1.18×10^{-4}	3.2×10^{-4}	1.53 ×	8.4×10^{-4}	
												10^2
		CR	0.1×10^{-6}	--	--	--	--	--	--	2.4 × 10^6	2.9×10^{-6}	
	2018-2019	HQ	2.2×10^{-3}	0.9×10^{-4}	2.8×10^{-4}	4.7×10^{-3}	0.2×10^{-4}	1.00×10^{-4}	2.9×10^{-4}	1.21 ×	7.3×10^{-4}	
												10^2
		CR	0.1×10^{-6}	--	--	--	--	--	--	1.87 ×	2.5×10^{-6}	
												10^6
	2019-2020	HQ	2.0×10^{-3}	0.8×10^{-4}	2.6×10^{-4}	3.3×10^{-3}	0.2×10^{-4}	0.7×10^{-4}	1.49×10^{-4}	0.9×10^{-2}	4.7×10^{-4}	
												10^6
		CR	0.1×10^{-6}	--	--	--	--	--	--	1.33 ×	1.61×10^{-6}	
												10^6
	Child	2017-2018	HQ	6.0×10^{-3}	2.6×10^{-4}	8.6×10^{-4}	1.11×10^{-3}	0.8×10^{-4}	2.9×10^{-3}	7.7×10^{-4}	3.7×10^{-2}	2.0×10^{-3}
												10^6
		CR	0.1×10^{-6}	--	--	--	--	--	--	1.44 ×	1.75×10^{-6}	
												10^6
2018-2019		HQ	5.3×10^{-3}	2.2×10^{-4}	6.7×10^{-4}	1.10×10^{-3}	0.6×10^{-4}	2.3×10^{-3}	7.1×10^{-4}	3.0×10^{-2}	1.77×10^{-3}	
												10^3
		CR	0.1×10^{-6}	--	--	--	--	--	--	1.14 ×	1.52×10^{-6}	
												10^6
2019-2020		HQ	4.8×10^{-3}	1.85×10^{-4}	6.3×10^{-4}	7.9×10^{-3}	0.5×10^{-4}	1.70×10^{-4}	3.6×10^{-4}	2.1×10^{-2}	1.14×10^{-3}	
												10^3
		CR	0.1×10^{-6}	--	--	--	--	--	--	0.8×10^6	1.0×10^{-6}	
												10^6

Table 3 Non-carcinogenic and carcinogenic risks for the deweathered element levels in PM_{2.5}.

Age	Year	Indicator	Cr	Mn	Fe	Co	Ni	Cu	Zn	As	Pb
Adult	2017-2018	HQ	3.1×10^{-3}	1.14×10^{-4}	3.8×10^{-4}	1.03×10^{-3}	0.5×10^{-4}	1.33×10^{-4}	3.2×10^{-4}	1.68×	1.08×
										10 ²	10 ³
		CR	0.2×10^{-6}	--	--	--	--	--	--	2.6×10 ⁶	3.7×10 ⁶
	2018-2019	HQ	2.7×10^{-3}	1.00×10^{-4}	3.1×10^{-4}	4.9×10^{-4}	0.4×10^{-4}	1.00×10^{-4}	2.9×10^{-4}	1.22×	6.9×10 ⁴
											10 ²
		CR	0.1×10^{-6}	--	--	--	--	--	--	1.89×	2.4×10 ⁶
2019-2020	HQ		2.5×10^{-3}	0.8×10^{-4}	3.0×10^{-4}	3.5×10^{-4}	0.4×10^{-4}	0.7×10^{-4}	1.49×10^{-4}	0.8×10^{-2}	4.1×10^4
	CR		0.1×10^{-6}	--	--	--	--	--	--	1.20×	1.40×
										10 ⁶	10 ⁶
Child	2017-2018	HQ	7.5×10^{-3}	2.8×10^{-4}	9.3×10^{-4}	1.17×10^{-3}	1.23×10^{-4}	3.2×10^{-4}	3.2×10^{-4}	4.1×10^{-2}	2.6×10^3
		CR	0.1×10^{-6}	--	--	--	--	--	--	1.58×	2.3×10 ⁶
	2018-2019	HQ	6.6×10^{-3}	2.3×10^{-4}	7.6×10^{-4}	1.19×10^{-3}	0.9×10^{-4}	2.4×10^{-4}	1.91×10^{-4}	3.0×10^{-2}	1.68×
											10 ³
		CR	0.1×10^{-6}	--	--	--	--	--	--	1.15×	1.44×
2019-2020	HQ	6.1×10^{-3}	1.99×10^{-4}	7.2×10^{-4}	8.4×10^{-4}	0.9×10^{-4}	1.71×10^{-4}	1.34×10^{-4}	1.89×	9.9×10^4	
										10 ²	
	CR	0.1×10^{-6}	--	--	--	--	--	--	0.7×10 ⁶	0.9×10 ⁶	

